Electrical and thermal control of Fabry-Pérot cavities mediated by Casimir forces

Lixin Ge ●,[*] Bingzhong Li, Hao Luo, and Ke Gong

School of Physics and Electronic Engineering, Xinyang Normal University, Xinyang 464000, China

Dynamic tuning of optical cavities is highly desired in many photonic systems. Here, we show that Fabry-Pérot (FP) cavities can be actively controlled by the Casimir force. The optical FP cavities consist of a gold nanoplate approaching to an electrical-connecting multilayer substrate in a liquid environment. The gold nanoplate can be stably suspended due to the balance of repulsive and attractive Casimir forces. Moreover, the suspension distance is modulated strongly by the electric gating or temperature of the system. As a result, we could shift the resonant wavelengths of the cavities with tens of nanometers at optical frequencies. Finally, we analyze the influence of Brownian motion on the equilibrium distances. Due to the high Q factor of the FP cavities, our proposed system offers a remarkable platform to experimentally investigate the thermal Casimir effect at submicrometer separations.

I. INTRODUCTION

The Casimir force between two perfect metallic plates, predicted by Hendrik Casimir in 1948, is a macroscopic quantum effect resulting from the zero-point fluctuations in vacuum [1]. Later, this quantum effect was generalized by E. M. Lifshitz to include frequency-dependent dielectrics and finite temperatures [2]. The Casimir forces between two objects consisting of the same materials are generally attractive. In the past two decades, great effort has been devoted to the search for Casimir repulsions in the vacuum environment [3–10], but there has been a lack of experimental verifications due to the strict constrains. By contrast, the Casimir repulsions have been experimentally achieved between two liquid-separated objects (labeled 1 and 2) when the permittivity satisfies $\varepsilon_1(i\xi) > \varepsilon_{\mathrm{liq}}(i\xi) > \varepsilon_2(i\xi)$ for a vast range of frequencies [11], where $\varepsilon_{\mathrm{liq}}(i\xi)$ is the permittivity of the intervening liquid evaluated with imaginary frequency $\omega = i\xi$. Interestingly, stable suspensions mediated by Casimir repulsions were reported in different configurations [12–17].

Recently, a new concept for tunable Fabry-Pérot (FP) cavities has been proposed by Esteso *et al.* [18], based on the Casimir force. The FP cavities play a crucial role in optical spectroscopy and find extensive applications [19]. For instance, the FP cavities consisting of metal-insulator-metal have received considerable interest in nanophotonics, due to their excellent performance in strong light-matter interactions [20–22]. In general, the resonances of FP cavities are fixed once the samples are fabricated [18]. The dynamic tuning of optical FP cavities through the Casimir force, particularly using external stimuli such as electric gating and temperature, remains largely unknown in this field.

Tunable Casimir forces can be realized by changing the dielectric response of the materials through external stimuli,

e.g., electric gating [23,24], magnetic fields [25–27], optical lasers [28,29], etc. Another scheme to dynamically tune the Casimir forces is based on the change of temperature [30–33]. Generally, thermal effect on the Casimir forces is weak [34,35]. For a vacuum gap, the thermal Casimir effect is observable only when the separation is large (e.g., over three micrometers) [35]. Such large separation severely affects its applications. Recently, a strong thermal Casimir effect based on graphene sheets was revealed at submicrometer scales [36–39]. The temperature dependence of Casimir forces for graphene is attributed to two different mechanisms. The first one is the thermal fluctuation, as illustrated by the implicit term in Ref. [40]. The second one relies on the fact that the dielectric response of graphene is temperature dependent (the explicit term in Ref. [40]). This kind of temperature modulation can be manifest at shorter separations.

In this study, we aim to dynamically tune FP cavities by manipulating the Casimir forces. Our system comprises a gold nanoplate and a Teflon-coated metal-oxide-semiconductor (MOS) substrate. Notably, the Casimir forces acting on the suspended gold nanoplate exhibit a strong dependence on both the gating voltage and the temperature. As a result, the equilibrium separation of the gold nanoplate undergoes significant alterations. The resonant wavelength of the optical FP cavities can be shifted for tens of nanometers. These remarkable shifts can be accurately detected using state-of-the-art experimental techniques. At the end, the Brownian motion of nanoplates is taken into account, and our study presents an accurate approach for measuring thermal Casimir forces at submicrometer separations via spectroscopy of the cavities.

II. THEORETICAL MODELS

Figure 1(a) illustrates the schematic of the system under study. In this setup, a gold nanoplate is suspended in a liquid of glycerol. The materials of Teflon, indium tin oxide (ITO), silica, and glycerol are almost transparent at optical frequen-
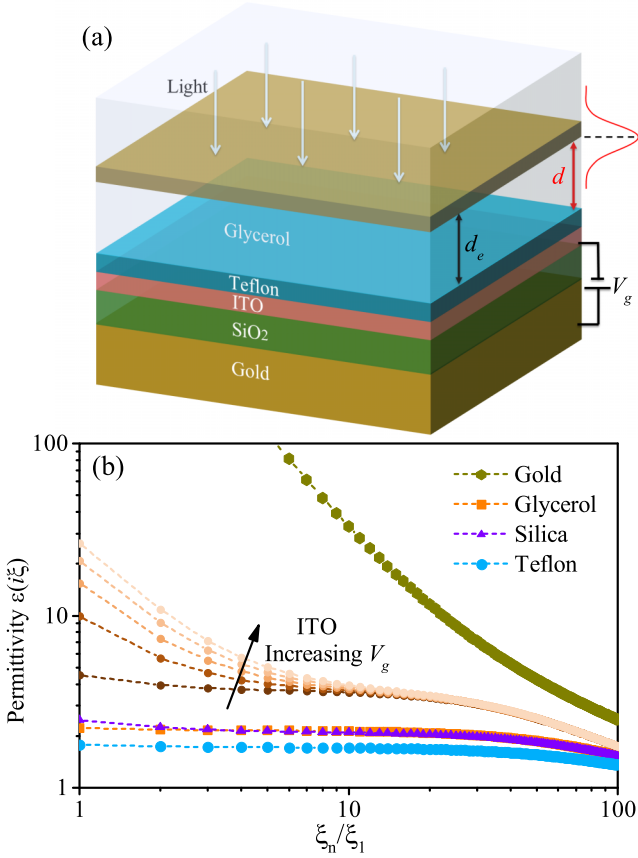
─────────
*[*]lixinge@hotmail.com

FIG. 1. (a) Schematic view of the system. The incident light is a plane wave, and the two parallel reflecting mirrors are consisted of the gold nanoplate and the gold substrate. We show the separation d is equal to the equilibrium distance d_e, which is generally the maximum probability of suspension high. The separation d could be fluctuated around the equilibrium distance due to the Brownian motion. (b) The dielectric response of materials evaluated in imaginary frequency. The plot depicts the permittivity of the accumulation layer of ITO, where the gating voltage increases from 0 to V_b with a step size of $V_b/4$.

cies. Hence, the two parallel reflecting mirrors of the optical FP cavities are the suspended gold nanoplate and the gold substrate. There exists an electrical connection between the gold substrate and the ITO layer, which can be controlled by a gating voltage.

Considering that the in-plane dimensions of the nanoplate is much larger than the separation d, a proximity force approximation is applied for the calculations. The Casimir force is calculated by $F_c = -\partial E_c(d)/\partial d$, where $E_c(d)$ is the Casimir energy between the nanoplate and the multilayer substrate [12]:

$$\frac{E_c(d)}{A} = k_b T \sum_{n=0}^{\infty}{}' \int \frac{d^2\mathbf{k}_\parallel}{(2\pi)^2} \ln \det[1 - \mathbf{R_1} \cdot \mathbf{R_2} e^{-2K_n d}], \quad (1)$$

where A represents the in-plane area, k_B is the Boltzmann constant, T is the temperature, d is the separation, the prime denotes a prefactor $1/2$ for $n = 0$, $\mathbf{k}_\parallel$ is the parallel wave vector, $K_n = \sqrt{k_\parallel^2 + \varepsilon_{liq}(i\xi_n)\xi_n^2/c^2}$ is the vertical wave vector

in the liquid, $\xi_n = 2\pi \frac{k_b T}{\hbar} n (n = 0, 1, 2, 3 \ldots)$ is the discrete Matsubara frequencies, $\hbar$ is the reduced Planck constant, and c is the speed of light in vacuum. $\mathbf{R}_{1,2}$ is the 2×2 reflection matrix, given by

$$\mathbf{R_j} = \begin{pmatrix} r_j^s & 0 \\ 0 & r_j^p \end{pmatrix}, \quad (2)$$

where r_j^α with $j = 1$ and $j = 2$ are the reflection coefficients for the upper and lower layered structures, and the superscripts $\alpha = s$ and p correspond to the polarization of transverse electric (**TE**) and transverse magnetic (**TM**) modes, respectively. The reflection coefficients are associated with the layer thicknesses and permittivity of materials, which can be calculated by a transfer matrix method (TMM) [41].

The generalized Drude-Lorentz model is applied for the gold [41]. The dielectric models and parameters for the materials of Teflon, silica, and glycerol are adopted from the recent literatures [42,43]. To fully describe the dielectric response of ITO, its permittivity is constructive by the sum of the Drude model and the Tauc-Lorentz model. For the Drude model, its expression is written as [44]

$$\varepsilon_D(\omega) = \varepsilon_\infty - \frac{\omega_p^2}{\omega^2 + i\omega\gamma_p}, \quad (3)$$

where we have $\varepsilon_\infty = 3.9$, $\gamma_p = 1.8 \times 10^{14}$ rad/s, $\omega_p = \sqrt{Ne^2/\varepsilon_o m^*}$ is the plasma frequency and N represents the magnitude of charge carrier density, e and ε_o denotes electron charge and the permittivity of vacuum, and $m^* = 0.35 m_e$ is the effective mass of charge carriers with m_e being the electron mass. For high frequencies above the band gap, the permittivity of ITO is given by the Tauc-Lorentz model [45,46]:

$$\varepsilon_{\text{TL}}(\omega) = i\Theta(\hbar\omega - E_g)\frac{A_{\text{TL}}C(\hbar\omega - E_g)^2}{\left(\hbar^2\omega^2 - E_0^2\right)^2 + (C\hbar\omega)^2}\frac{E_0}{\hbar\omega}, \quad (4)$$

where $\Theta(x)$ is the Heaviside step function; the fitting parameters are [47] $A_{\text{TL}} = 111.4$ (eV), $C = 11.7$ (eV), and $E_0 = 9.6$ (eV); and the band gap of ITO is $E_g = 3.13$ (eV). Then, the permittivity for the ITO material, i.e., $\varepsilon(i\xi_n)$, can be calculated by the Kramers-Kronig relationship, wherein the absorptions from both the Drude model and the Tauc-Lorentz model are taken into account.

When a voltage is applied, it alters the distribution of carriers in the ITO nanofilm. This is due to the gate-induced electrical field, which penetrates the insulating layer and attracts the carriers to accumulate at or compel away from the ITO-insulator interface. This depends on the types of carriers in the ITO and the direction of gating. Consequently, the ITO layer can be categorized into two distinct regions: the background layer and the active layer. The carrier densities in these two layers are denoted as N_b and N_a, respectively. The magnitude of N_b is fixed upon fabrication, whereas the magnitude of N_a can be adjusted by varying the gating voltage. As given in previous literatures, the active layer possesses a homogeneous carrier density, and its thickness is determined
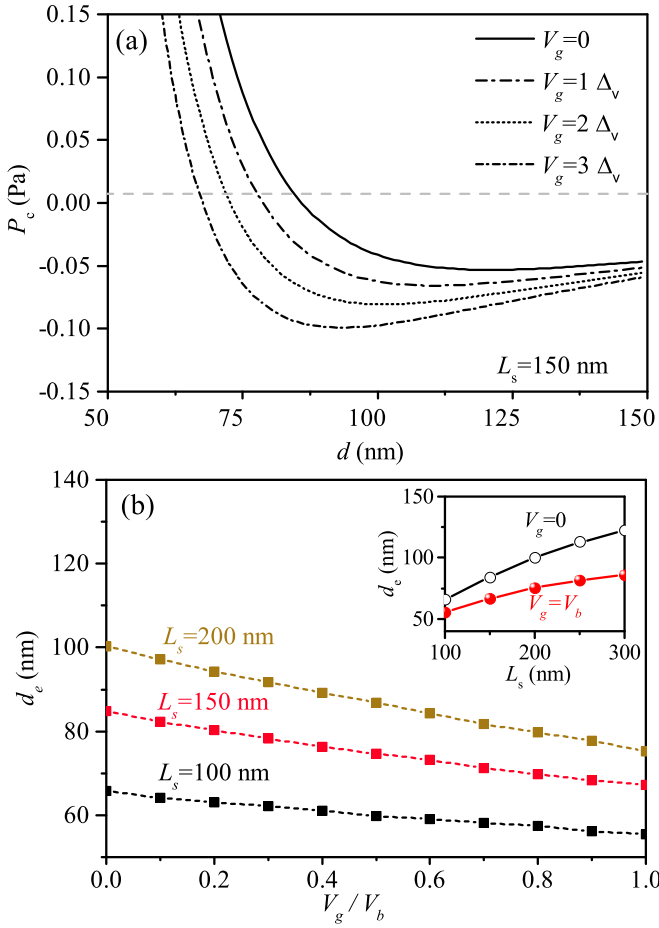
FIG. 2. (a) Casimir pressures under different gating voltages, where $\Delta_v = V_b/3$, where the breakdown voltage is 450 V. The positive (negative) sign of the pressure corresponds to the repulsive (attractive) force. The gray dashed line represents the pressure generated from the gravity and buoyancy. (b) Equilibrium distances as a function of applied voltages. The inset shows the equilibrium distances as a function of the thickness of silica layer.

by [24,48]

$$L_a = \frac{\pi}{\sqrt{2}} \sqrt{\frac{k_B T \varepsilon_0 \varepsilon_{ITO}}{N_b e^2}}, \tag{5}$$

where $\varepsilon_{ITO} = 9.3$ is the static permittivity of ITO. It is assumed that the carrier density N_a is uniform across the thickness L_a, although in real configurations it exhibits nonuniformity. Therefore, for this assumption to hold, the separation d should be significantly larger than the thickness L_a. Here, the thickness of the ITO layer is fixed to be 5 nm, and the background carrier density $N_b = 10^{19}$ cm^{-3}. We have $L_a = 2.56$ nm at $T = 300$ K. On the other hand, the analytical expression of N_a is given by [24]

$$N_a = N_b + \frac{\varepsilon_0 \varepsilon_s V_g}{e L_s L_a}, \tag{6}$$

where $\varepsilon_s = 3.9$ denotes the static dielectric constant of silica and V_g is the applied voltage, which should be smaller than the breaking down voltage $V_b = E_b L_s$, where we assume the breakdown field $E_b = 30$ MV/cm [49,50]. Note that the
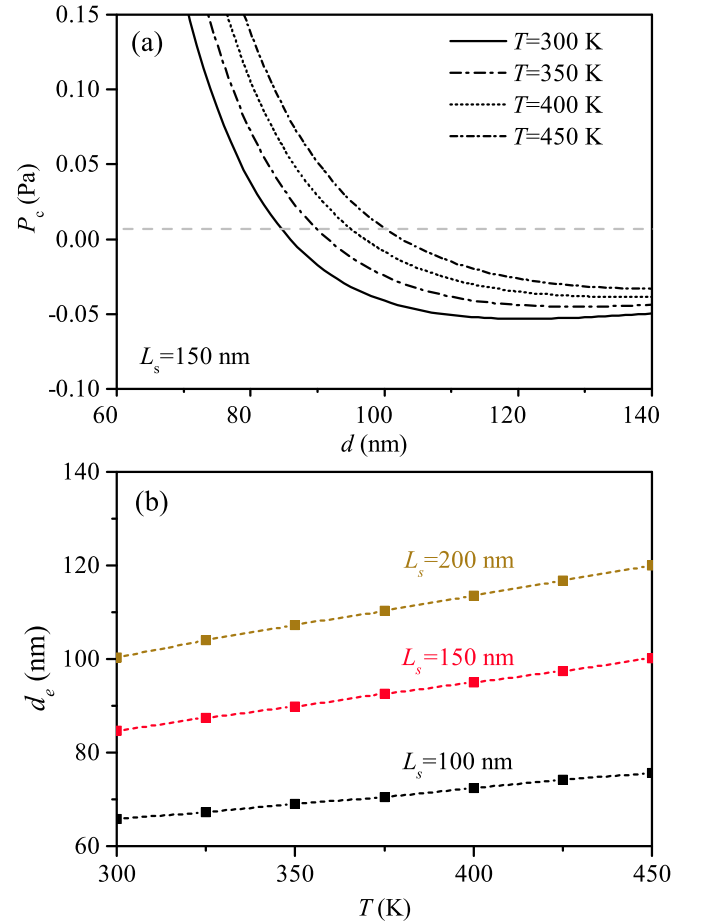

FIG. 3. (a) Casimir pressures for different temperatures, where there is no applied voltage. The gray dashed line represents the pressure generated from the gravity and buoyancy. (b) Equilibrium distances as a function of temperature.

carrier density N_a in the active layer increases monotonously with the positive gating voltage. For negative configuration with gating voltage V_g changing from 0 to -V_b, the carrier density N_a would be depleted gradually to zero. Then, it changes sign from positive to negative (i.e., from electron doping to hole doping) for a large reverse gating, wherein the inversion layer presents. To demonstrate electric-gating modulation of the Casimir effect, we are mainly focused on a positive gating in this work, and the active layer corresponds to the accumulation layer.

The permittivity evaluated in the imaginary frequency is presented in Fig. 1(b). Notably, the dielectric functions of the ITO in the accumulation layer exhibit significant variations with increasing voltages in the infrared frequency range. Teflon possesses the lowest permittivity, making it particularly desirable for Casimir repulsions at small separations. Although the permittivity of glycerol is close to that of silica at infrared and visible frequencies, its static permittivity, about 42.4, at zero frequency is much larger than that of silica.

III. RESULTS AND DISCUSSION

The Casimir pressure of the suspended gold nanoplate versus the separation is shown in Fig. 2(a). The thickness of
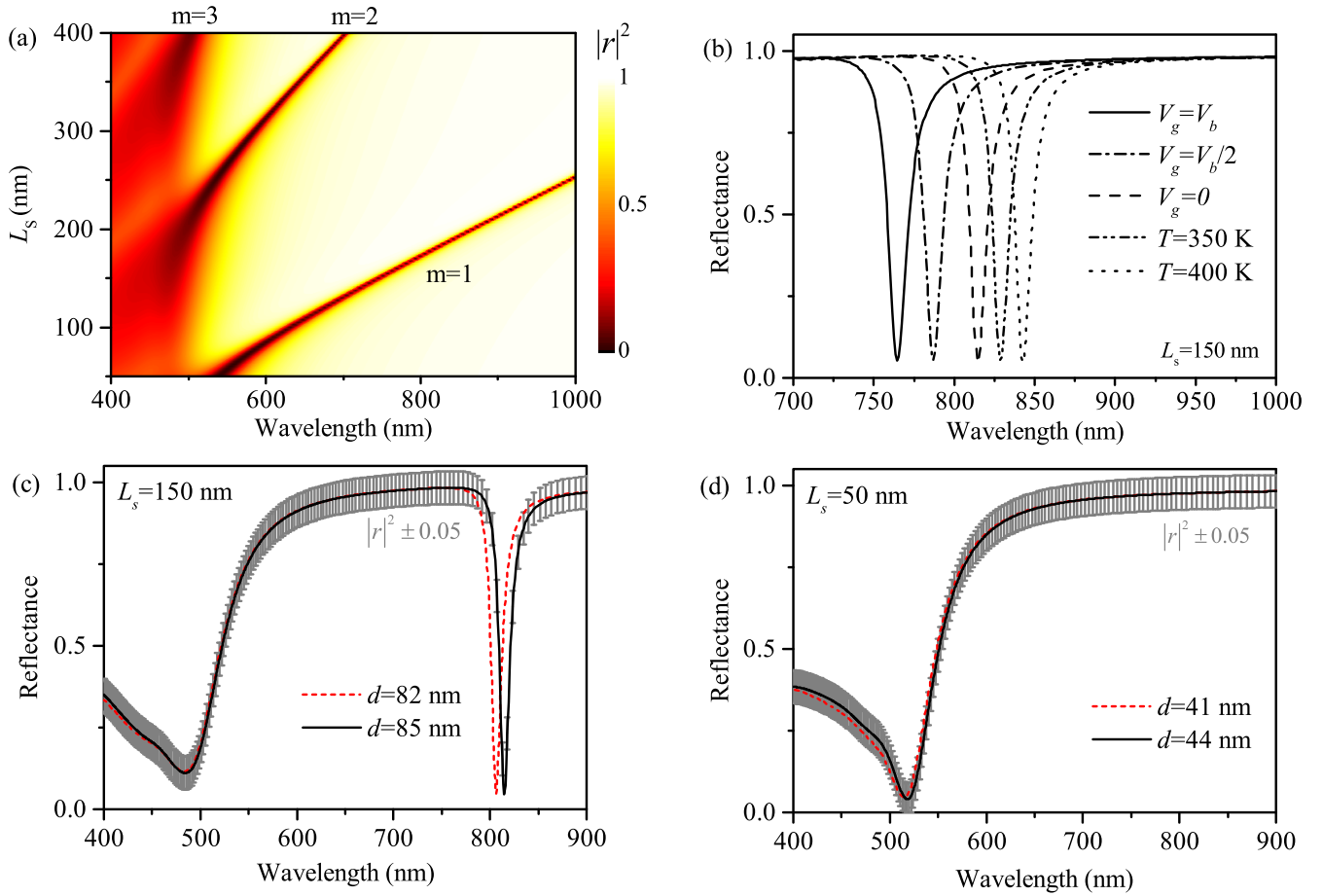
FIG. 4. (a) The reflectance of FP cavity varies with the layer thickness of silica, where the separation d is fixed at 60 nm. (b) The modulation of reflectance through the applied voltage and temperatures. (c and d) Reflection spectra in and out of the equilibria. The equilibrium distances for $L_s = 150$ nm and $L_s = 50$ nm are 85 nm and 44 nm, respectively. The assumed error of the reflectance with ± 0.05 is given for the equilibrium separation represented by the gray bars.

the gold nanoplate, Teflon, ITO, and silica layers are set to be 40, 10, 5, and 150 nm, respectively. The results demonstrate a significant modulation of the Casimir pressure by the gating voltage. At small separations, the Casimir pressure is repulsive, while it turns to be an attractive force for larger separations. A separation for zero pressure, known as the Casimir equilibrium, is identified at a specific separation. With increasing the voltage, the pressure tends to be attractive, and the separation for the Casimir equilibrium decreases correspondingly. In the absence of voltage, the Casimir equilibrium appears at approximately 85 nm, which decreases by about 18 nm as the voltage approaches to V_b. For a gold nanoplate with thickness of 40 nm, the pressure resulting from gravity and buoyancy is estimated to be 0.007 Pa [41], and is represented by the dashed gray lines in Fig. 2(a). The equilibrium distance, denoted as d_e, is established through the delicate balance among the Casimir force, gravity, and buoyancy. The d_e is slightly smaller than the separation of Casimir equilibrium.

The equilibrium distance as a function of applied voltage is depicted in Fig. 2(b). The findings demonstrate a decline in the equilibrium distance as the voltage increases, ranging from 0 up to V_b. The equilibrium distance is also influenced by the thickness of the silica layer, as shown for $L_s = 100$, 150, and 200 nm. The inset of Fig. 2(b) reveals that increasing

the layer thickness results in elevated equilibrium distances, and the difference of d_e between $V_g = 0$ and $V_g = V_b$ expands. At $L_s = 300$ nm, the difference of d_e for the $V_g = 0$ and $V_g = V_b$ reaches nearly 36 nm. The calculations suggest that the equilibrium distance, and thus the resonant length, of the FP cavities can be effectively modulated by the tunable Casimir forces through electrical gating.

The Casimir pressure is also strongly dependent on the temperature, as shown in Fig. 3(a). The layer thicknesses of the materials are kept the same as those in Fig. 2(a). To manifest the temperature effect on the Casimir force, the applied voltage is assumed to be zero. We find that the Casimir pressure tends to be more repulsive as the temperature increases, and the variation of d_e is near 10 nm when the temperature increases from 300 to 400 K. The Casimir pressure as a function of temperature is shown in Fig. 3(b) under different L_s. Again, the value of d_e increases when the layer thickness L_s increases from 100 to 200 nm. The variation of d_e with respect to T is almost linear as reported in Ref. [51]. Such effective modulation of d_e due to the temperature has been proposed for detection of thermal Casimir effect [52]. However, the optical resonances have not been employed in the literature [51,52].

The thickness of silica needs to be carefully designed. The contour plot of the reflectance via silica thickness and

wavelength λ is shown in Fig. 4(a), wherein the separation d is fixed at 60 nm. The reflectance is calculated by the TMM in the real frequency [53]. The results reveal that different resonant modes are excited when the thickness L_s varies from 50 to 400 nm. A fundamental mode with $m = 1$ is excited in the visible regime when the layer thickness L_s is in the proper range. As the thickness increases to a higher value, e.g., 300 nm, other high-order modes are presented.

Figure 4(b) shows the reflection spectra under different external stimuli, where the nanoplate is suspended at the equilibrium distance d_e. The resonance of the FP cavities is modulated efficiently by the applied voltage and temperature. The equilibrium distances are about 85, 75, and 67 nm for the applied voltages of 0, $V_b/2$, and V_b, respectively. On the other hand, the equilibrium distances increase to 90 and 95 nm for the temperatures 350 and 400 K, respectively. Hence, the resonant dip has a blue shift for increasing the voltages, while it has a red shift for increasing the temperature. The results show that the giant shifting of the resonances over tens of nanometers is achieved by electrical gating or temperatures.

In a real configuration, the imperfection of the experiments (e.g., misalignment, surface roughness, electrostatic forces, etc.) may exist, and the errors of the reflectance with ± 0.05 (gray error bars) should be introduced as indicated in Ref. [18]. Here, the high Q factor of optical cavities provides an avenue for accurate spectroscopic measurements. For instance, the resonant wavelength without the electrical gating appears at about 810 nm, where the equilibrium separation is 85 nm. When the separation is out of equilibrium with $d = 82$ nm, the resonant wavelength can be clarified by the spectroscopy, as shown in Fig. 4(c). The calculated results indicate that such small errors have limited influence as long as the spectra have high Q factors. For thickness $L_s = 50$ nm, the equilibrium separation is 44 nm, and the shift of the reflection spectrum could not be clarified in Fig. 4(d). This is because the resonance of the cavities appears at the lossy regime (λ is smaller than about 550 nm) with $L_s = 50$ nm, and the change of reflection spectrum due to the variation of separation could not be detected by the spectroscopy at such a configuration.

The Brownian motion should be considered when the suspended nanoplate is finite size. The random Brownian motion happens at both lateral and vertical directions. The lateral Brownian motion does not affect the optical resonances of FP cavities. However, the vertical Brownian motion could make the stable suspension of nanoplates out of equilibrium. The normalized probability of the suspension distance due to the vertical Brownian effect is given by [54]

$$\rho(d, T) = \frac{\mathrm{Exp}[-U(d)/k_B T]}{\int_0^\infty \mathrm{Exp}[-U(d)/k_B T]\partial d}, \qquad (7)$$

where $U(d) = E_c(d) + F_{\mathrm{GB}}d$ is the total energy of the suspended nanoplate, where F_{GB} is the sum of the gravity and buoyancy forces [41,54]. Here, we consider the gold nanoplate with area $A = 20\,\mu\mathrm{m} \times 20\,\mu\mathrm{m}$ (see the experiment samples in Ref. [12]). The normalized probability with respect to the separation is shown in Figs. 5(a) and 5(b), where we set $L_s = 300$ and 150 nm, respectively. The higher the probability
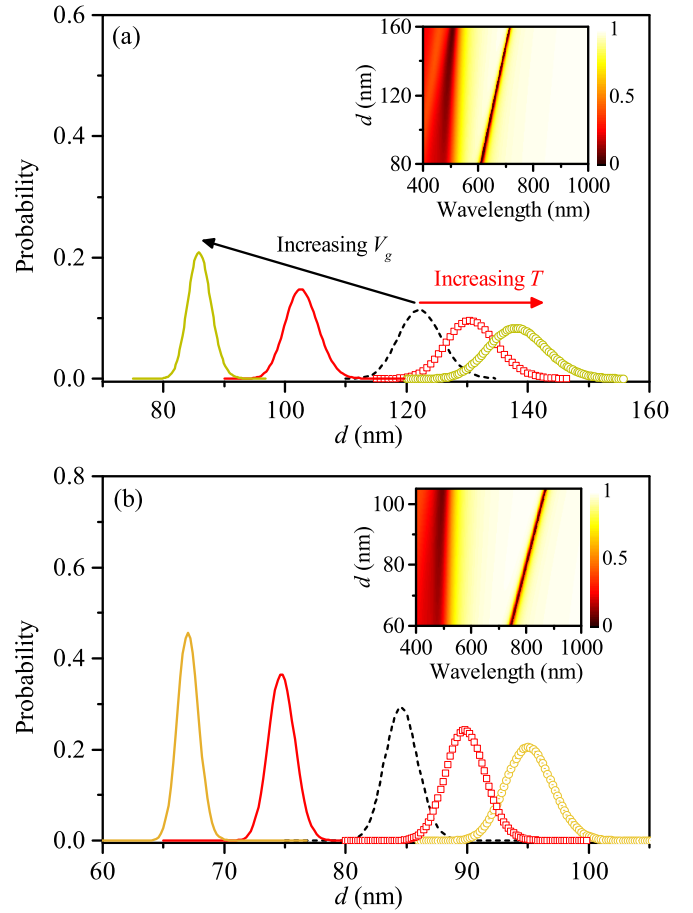

FIG. 5. The probability of suspension positions due to the Brownian effect with (a) $L_s = 300$ nm and (b) $L_s = 150$ nm. The increasing voltages are 0, $V_b/2$, and V_b. The increasing temperatures are 300, 350, and 400 K. The dashed lines represent the initialing state with $V_g = 0$ and $T = 300$ K. The insets in (a) and (b) show the corresponding contour maps of the reflectance.

at the equilibrium distance, the narrower the suspension distribution. The peak probability $\rho(d_e, T)$ for $L_s = 150$ nm is almost two times larger than that of $L_s = 300$ nm, indicating a stronger stiffness at the quantum trapping. Overall, the probability $\rho(d_e, T)$ increases with increasing the applied voltage. By contrast, the probability $\rho(d_e, T)$ decreases slightly with increasing the temperature from 300 to 350 and 400 K. The distribution functions could be overlapping with each other at an intervening 50 K. The average of separations would be [54]

$$\bar{d} = \frac{\int_0^\infty d\,\mathrm{Exp}[-U(d)/k_B T]\partial d}{\int_0^\infty \mathrm{Exp}[-U(d)/k_B T]\partial d} \qquad (8)$$

The $\bar{d}$ is obtained by averaged over multiple measurements [12]. The offset value $\triangle = \bar{d} - d_e$ is generally smaller than 1 nm for area $A = 20\,\mu\mathrm{m} \times 20\,\mu\mathrm{m}$, due to the symmetry of the probability function near the equilibrium distance. The precise measurement of the thermal Casimir effect relies on the suspended separation of the nanoplate. Fortunately, the high Q spectra in optical cavities offer an opportunity to monitor the separation accurately. As depicted in the insets of Figs. 5(a) and 5(b), the high Q factor is maintained over a wide range

of separations. Compared with previous literature [51,52], our work presents an accurate way to detect thermal Casimir effect via spectroscopic measurements of optical cavities.

IV. CONCLUSIONS

The optical FP cavities tuned by the Casimir forces are investigated in this work. The system consists of a gold nanoplate approaching to a Teflon-coated MOS substrate in a liquid environment. The suspension of the gold nanoplate is dependent on the balance among the Casimir, gravity, and buoyancy forces. One way to modulate the suspension distance of the gold nanoplate is achieved by electrical gating. With increasing the positive voltages from 0 to V_b, the pressure tends to be attractive, and the separation for the Casimir equilibrium decreases correspondingly due to the accumulation of carrier density at the active region. The frequency shifting of the reflection spectra can be tens of nanometers via gating voltages. Furthermore, the control of the optical resonances via the temperature is also demonstrated. The temperature modulations can be manifested greatly at sub-micrometer separations. In addition, the Brownian motion is discussed in different configurations. A different scheme to measure thermal Casimir effect is suggested by the spectroscopic measurements of the optical FP cavities.

It is worth mentioning that we only consider the case of carrier accumulation with positive gating, in order to prove the concept of gate-tunable FP cavities. While the carrier in the active layer could be depleted or even reversed for a negative gating, it can be easy to predict that the separation for the Casimir equilibrium would increase, due to the depletion of carrier density at the active region. When inversion presents, the active layer consists of an inversion layer and depleting layer in a real configuration, which makes the calculated model more complicated. The quantity study of Casimir force (as well as the tunable FP cavities) for negative gating would be one of the interesting directions in future works.

[1] H. B. G. Casimir, Proc. Kon. Ned. Akad. Wet. **51**, 793 (1948).

[2] E. M. Lifshitz, J. Exper. Theoret. Phys. USSR **29**, 94 (1956) [Sov. Phys.-JETP **2**, 73 (1956)].

[3] L. M. Woods, D. A. R. Dalvit, A. Tkatchenko, P. Rodriguez-Lopez, A. W. Rodriguez, and R. Podgornik, Rev. Mod. Phys. **88**, 045003 (2016).

[4] O. Kenneth, I. Klich, A. Mann, and M. Revzen, Phys. Rev. Lett. **89**, 033001 (2002).

[5] R. Zhao, J. Zhou, T. Koschny, E. N. Economou, and C. M. Soukoulis, Phys. Rev. Lett. **103**, 103602 (2009).

[6] M. Levin, A. P. McCauley, A. W. Rodriguez, M. T. Homer Reid, and S. G. Johnson, Phys. Rev. Lett. **105**, 090403 (2010).

[7] P. Rodriguez-Lopez and A. G. Grushin, Phys. Rev. Lett. **112**, 056804 (2014).

[8] W. Nie, R. Zeng, Y. Lan, and S. Zhu, Phys. Rev. B **88**, 085421 (2013).

[9] Z. Li and C. Khandekar, Phys. Rev. Appl. **16**, 044047 (2021).

[10] M. Camacho, T. Gong, B. Spreng, I. Liberal, N. Engheta, and J. N. Munday, Phys. Rev. A **105**, L061501 (2022).

[11] J. N. Munday, F. Capasso, and V. A. Parsegian, Nature (London) **457**, 170 (2009).

[12] R. Zhao, L. Li, S. Yang, W. Bao, Y. Xia, P. Ashby, Y. Wang, and X. Zhang, Science **364**, 984 (2019).

[13] M. Dou, F. Lou, M. Boström, I. Brevik, and C. Persson, Phys. Rev. B **89**, 201407(R) (2014).

[14] V. Esteso, S. Carretero-Palacios, and H. Míguez, J. Phys. Chem. C **119**, 5663 (2015).

[15] X. Liu and Z. M. Zhang, Phys. Rev. Appl. **5**, 034004 (2016).

[16] Y. Ye, Q. Hu, Q. Zhao, and Y. Meng, Phys. Rev. B **98**, 035410 (2018).

[17] V. Esteso, S. Carretero-Palacios, and H. Míguez, J. Phys. Chem. Lett. **13**, 4513 (2022).

[18] V. Esteso, S. Carretero-Palacios, and H. Míguez, J. Phys. Chem. Lett. **10**, 5856 (2019).

[19] J. M. Vaughan, *The Fabry–Perot Interferometer: History, Theory, Practice and Applications* (Routledge, Oxfordshire, 2017).

[20] V. Caligiuri, G. Biffi, M. Palei, B. Martín-García, R. D. Pothuraju, Y. Bretonnière, and R. Krahne, Adv. Opt. Mater. **8**, 1901215 (2020).

[21] N. Liu, M. Mesch, T. Weiss, M. Hentschel, and H. Giessen, Nano Lett. **10**, 2342 (2010).

[22] H. Deng, Z. Li, L. Stan, D. Rosenmann, D. Czaplewski, J. Gao, and X. Yang, Opt. Lett. **40**, 2592 (2015).

[23] L. Ge, X. Shi, L. Liu, and K. Gong, Phys. Rev. B **102**, 075428 (2020).

[24] T. Gong, B. Spreng, M. Camacho, I. Liberal, N. Engheta, and J. N. Munday, Phys. Rev. A **106**, 062824 (2022).

[25] Q.-D. Jiang and F. Wilczek, Phys. Rev. B **99**, 125403 (2019).

[26] R. Zeng and Y. Yang, Phys. Rev. A **83**, 012517 (2011).

[27] J. Wang, X. Zhang, S.-Y. Pei, and D.-H. Liu, Phys. Rev. A **73**, 042103 (2006).

[28] F. Chen, G. L. Klimchitskaya, V. M. Mostepanenko, and U. Mohideen, Phys. Rev. B **76**, 035338 (2007).

[29] C.-C. Chang, A. A. Banishev, G. L. Klimchitskaya, V. M. Mostepanenko, and U. Mohideen, Phys. Rev. Lett. **107**, 090403 (2011).

[30] V. A. Yampol'skii, S. Savel'ev, Z. A. Mayselis, S. S. Apostolov, and F. Nori, Phys. Rev. Lett. **101**, 096803 (2008).

[31] E. G. Galkina, B. A. Ivanov, S. Savel'ev, V. A. Yampol'skii, and F. Nori, Phys. Rev. B **80**, 125119 (2009).

[32] M. Boström, M. Dou, O. I. Malyi, P. Parashar, D. F. Parsons, I. Brevik, and C. Persson, Phys. Rev. B **97**, 125421 (2018).

[33] L. Ge and X. Shi, Phys. Lett. A **450**, 128392 (2022).

[34] M. Boström and B. E. Sernelius, Phys. Rev. Lett. **84**, 4757 (2000).

[35] A. Sushkov, W. Kim, D. Dalvit, and S. Lamoreaux, Nat. Phys. **7**, 230 (2011).

[36] M. Liu, Y. Zhang, G. L. Klimchitskaya, V. M. Mostepanenko, and U. Mohideen, Phys. Rev. B **104**, 085436 (2021).

[37] C. Abbas, B. Guizal, and M. Antezza, Phys. Rev. Lett. **118**, 126101 (2017).

[38] G. Bimonte, G. L. Klimchitskaya, and V. M. Mostepanenko, Phys. Rev. A **96**, 012517 (2017).

[39] N. Khusnutdinov, R. Kashapov, and L. M. Woods, 2D Mater. **5**, 035032 (2018).

[40] G. L. Klimchitskaya and V. M. Mostepanenko, Phys. Rev. B **91**, 174501 (2015).

[41] L. Ge, X. Shi, Z. Xu, and K. Gong, Phys. Rev. B **101**, 104107 (2020).

[42] M. Moazzami Gudarzi and S. H. Aboutalebi, Sci. Adv. **7**, eabg2272 (2021).

[43] H. S. Sehmi, W. Langbein, and E. A. Muljarov, Phys. Rev. B **95**, 115444 (2017).

[44] A. V. Krasavin and A. V. Zayats, Phys. Rev. Lett. **109**, 053901 (2012).

[45] G. Jellison, Jr. and F. Modine, Appl. Phys. Lett. **69**, 371 (1996).

[46] A. A. Banishev, C.-C. Chang, R. Castillo-Garza, G. L. Klimchitskaya, V. M. Mostepanenko, and U. Mohideen, Phys. Rev. B **85**, 045436 (2012).

[47] H. Fujiwara and M. Kondo, Phys. Rev. B **71**, 075109 (2005).

[48] F. Yi, E. Shim, A. Y. Zhu, H. Zhu, J. C. Reed, and E. Cubukcu, Appl. Phys. Lett. **102**, 221102 (2013).

[49] G. T. Papadakis and H. A. Atwater, Phys. Rev. B **92**, 184101 (2015).

[50] C. Sire, S. Blonkowski, M. J. Gordon, and T. Baron, Appl. Phys. Lett. **91**, 242905 (2007).

[51] V. Esteso, S. Carretero-Palacios, and H. Míguez, J. Appl. Phys. **119**, 144301 (2016).

[52] A. W. Rodriguez, D. Woolf, A. P. McCauley, F. Capasso, J. D. Joannopoulos, and S. G. Johnson, Phys. Rev. Lett. **105**, 060401 (2010).

[53] T. Zhan, X. Shi, Y. Dai, X. Liu, and J. Zi, J. Phys.: Condens. Matter **25**, 215301 (2013).

[54] J. Varela, A. W. Rodriguez, A. P. McCauley, and S. G. Johnson, Phys. Rev. A **83**, 042516 (2011).